Simulation of Flow-induced Multi-particle Motion with FEM-based Method

Xiaobo Peng[1] , Diwei Zhang[2] , Dongdong Zhang[3] and Lai Jiang[4]

[1]Prairie View A&M University, xipeng@pvamu.edu
[2]Prairie View A&M University, zhang.diwei@yahoo.com
[3]Prairie View A&M University, peterzdd_2002@hotmail.com
[4]Prairie View A&M University, laijiang@pvamu.edu

Corresponding author: Xiaobo Peng, xipeng@pvamu.edu

Abstract. This paper presents a finite element based explicit fluid-structure coupling method. The derived method is proposed to solve flow-induced multi-particle motion in the low Reynolds number flow. The particle motion is treated as a non-linear geometric dynamic problem. The Total-Lagrangian finite element method is applied to describe and discretize the particle domain. The Bathe method is used to integrate over the time domain. The quasi-steady Stokes equation is used as the governing equation of the fluid domain. Mixed finite element is applied to solve the fluid equation. An explicit coupling strategy is implemented between the interaction of particle and the zero-Reynolds number flow. Simulations of the flow-induced multi-particle motion with derived method are presented.

Keywords: flow-induced multi-particle motion, Finite element method, fluid-structure interaction

1   INTRODUCTION

Flow induced multi-particle motion is a common phenomenon which can be found in different areas. Particle immersed in the flow with low-Reynolds number is a main characteristic of this kind of problems. Motions of particles, such as translation, rotation, deformation, interaction between wall and particles, and interaction among particles are complicated problems. Studying motions of particles may reveal insights of multi-particle motion phenomenon and also benefit several different industries. To manufacture the short-fiber reinforced composite material using injection molding process, fibers immersed in the resin matrix are injected into the mold. Fiber's motions including transport, rotation, and deformation are subject to the motion of the fluid. The final distribution and pattern of fibers determines the performance of final products. Similarly, in the paper making industry, pulp with paper fiber in the processing of forming paper is a flow induced fiber motion problem. In the medical application, blood cell motion in the blood vessel also can be categorized

into this field. Obtaining insight of physical meaning of blood cell motion may be helpful for understanding mechanism behind some diseases from different perspective.

The goal of this research is to derive a computational method to simulate the low Reynolds number flow-induced particle motion problem. The derived method is able to address the different shape of particles. It is also able to simulate rigid particles and flexible particles. The quasi-static Stokes equation was applied as the governing equation of the fluid domain which was solved by the finite element method. The particle was treated as a non-linear geometric problem. The Total-Lagrangian (TL) finite element was used to discretize the particle. The Bathe method was applied to integrate the particle's dynamic motion over the time domain. A serial partitioned coupling method was derived to couple the fluid and solid domains [12].

The derived method is validated by comparing simulation results with the Jeffery theory. Behaviors of different geometry and aspect ratio of particles are compared with simulation. Simulation of three rectangular particles immersed in the double Couette flow with the derived method is presented. Characteristics of multi-particle motion particle are discussed. Influence of initial position of three particles on the behavior of the particles' motion is also discussed.

2   LITERATURE REVIEW

Jeffery [6] developed a mathematical formula to describe an orbit of a rigid ellipsoid particle immersed in the shear flow. Zero inertia of both fluid and particle was an assumption. Fluid domain is assumed infinite large to avoid boundary effect on the motion of the particle. Jeffery's theory is the foundation of theoretical works concerning this problem. Two-dimensional Jeffery theory is described in Eq. (2.1).

$$\emptyset(t) = tan^{-1}(r_e tan \frac{\dot{\gamma}t}{r_e + 1/r_e}) \tag{2.1}$$

Fiber's rotation angle $\emptyset$ is a time-dependent variable. Ellipsoid aspect ratio is represented by r_e. Time t is the variable of the equation. Flow shear rate $\dot{\gamma}$ can be calculated by equation $\dot{\gamma} = V_c/L$, where V_c is the characteristic velocity and L is the height of simple shear flow. Figure 1 illustrates an ellipsoid fiber immersed in a double Couette flow and the mentioned notations applied in Jeffery's theory.
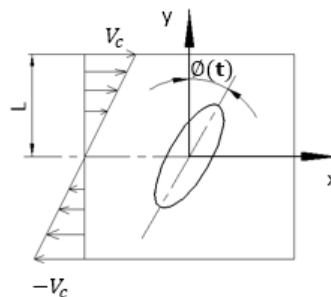

Figure 1: An illustration of an ellipsoid fiber immersed in the double Couette flow.

Jeffery's theory reveals that fiber's angular velocity increases with the increase of flow shear rate. An ellipsoid fiber's angular velocity reaches the maximum while the fiber's long axis orientation is perpendicular to the flow shear direction. An ellipsoid fiber's angular velocity reduces to the minimum while the fiber's long axis orientation is parallel to flow shear direction.

Most of the theoretical works regarding flow-induced rigid particle motion are the extension of Jeffery's theory. In Ho and Leal's [5] study, non-Newtonian effect and weak inertial of fluid were involved. It was concluded that axisymmetric but non-spheroid particles generally show the same

behavior in the shear flow as a spheroid particle. Stover and Cohen's [11] experimental results agreed with Jeffery's theory and Leal's theory quantitatively.

For the multi-particle motion, Folgar and Tucker III [4] derived an orientation distribution function of the concentrated suspensions. Even though their theory predicted more rapid alignment than actual is, it has been widely used and modified in the simulation of the injection molding of short fiber composite material. This method has its limitation which is only able to solve rigid slender shape fiber motion. It is unable to solve the particle with arbitrary geometry or the flexible fiber.

Arbitrary-Lagrangian-Eulerian (ALE) [3] is used widely as a computational method for solving fluid-structure interaction problem. The mesh of an ALE kinematical description of the fluid domain can displace independently of the fluid motion. The ALE improves accuracies of the calculation and alleviates excessive distortion of the computational mesh. For the flow-induced particle motion problem, however, large translation and rotation occur in the computation. The ALE is incapable to withstand very large computational mesh displacement, and re-mesh is inevitable. Transformation of data from the previous mesh to the current mesh is a tedious work in which accuracy of calculation is compromised.

Immersed Boundary (IB) method [8] is another computational solution in which the fluid applies a fixed space, the Eulerian description. The mesh of the fluid is no longer moved to confirm the surface of the particle. Two domains are linked by an interaction equation which is named 'the Dirac delta function'. Moving mesh and re-mesh are avoided in the IB method. Nonetheless, the accuracy of the IB method is not better than methods with the conformed interface between the two domains.

3   METHOD

Flow-induced multi-particle motion was studied with numerical method in this paper. Problem was limited in the low Reynolds number flow. Amount of particle was limited in three. Problem was simplified in the two-dimension. In this section, we will discuss the modeling and solution of the zero Reynolds number flow and multi-particle motion, coupling strategy and re-mesh scheme.

3.1   Zero-Reynolds Number flow

Since the size and weight of the fiber that we are dealing with are quite small, so we assume a zero-Reynolds number-flow in this study. And the Stokes equation is used as the governing equation of the fluid domain.

$$\boldsymbol{\nabla} \cdot \mathbf{V} = 0 \tag{3.1}$$

$$-\boldsymbol{\nabla} \cdot \{-p\mathbf{I} + [(\boldsymbol{\nabla}\mathbf{V}) + (\boldsymbol{\nabla}\mathbf{V})^T])\} = 0 \tag{3.2}$$

where p is pressure distribution and $\mathbf{V}$ is the velocity distribution vector. For the two-dimensional case, $\mathbf{V} = \{u, v\}$, where u is the velocity distribution in the x-direction and v is the velocity distribution in the y-direction.

Equation (3.1) and (3.2) are time-independent equation representing a quasi-static problem. Solving a quasi-static Stokes equation is easier and faster than solving a dynamic Navier-Stokes equation. An acceptable accuracy can be obtained in the solving low Reynolds number problem with Stokes equation compared to that applying a Navier-Stokes equation.

According to the Ladyzhenskaya-Babuska-Breezi (LBB) condition which is also known as the inf-sup condition [10], the interpolation function of the pressure should be one order low than the interpolation function of the velocity based on the differential order of each term in the governing equation. Therefore, the mixed finite element is applied to solve Eq. (3.1) and Eq. (3.2) simultaneously. The Galerkin finite element method discretizes the governing equation from the strong form to the weak form. Integration of multiplication of residual of governing equation and weight function is shown in Eq. (3.3) to Eq. (3.5). They are mass conservation, momentum conservation in the x-direction, and momentum conservation in the y-direction, sequentially.

$$\int_{\Omega} \left\{ \frac{\partial u}{\partial x} + \frac{\partial v}{\partial y} \right\} Q dx dy = 0 \tag{3.3}$$

$$\int_{\Omega} \left\{ -\frac{\partial}{\partial x}\left[-p + 2\frac{\partial u}{\partial x}\right] - \frac{\partial}{\partial y}\left[\frac{\partial v}{\partial x} + \frac{\partial u}{\partial y}\right] \right\} w dx dy = 0 \tag{3.4}$$

$$\int_{\Omega} \left\{ -\frac{\partial}{\partial x}\left[\frac{\partial v}{\partial x} + \frac{\partial u}{\partial y}\right] - \frac{\partial}{\partial y}\left[-p + 2\frac{\partial v}{\partial y}\right] \right\} w dx dy = 0 \tag{3.5}$$

In Eq. (3.3) to Eq. (3.5), u and v represent fluid velocity in the x-direction and in the y-direction. Terms Q and w are different weighting function [10]. Distmesh, a free mesh tool [7], was applied to discretize the geometry of the fluid domain. Finally, discretized governing equations can be written into a matrix form, as shown in Eq. (3.6).

$$K_f \cdot X(V_x, V_y, P) = F(F_x, F_y) \tag{3.6}$$

Herein, K_f is stiffness matrix generated by the mixed finite element method. $X(V_x, V_y, P)$ represents known and unknown values vector, where V_x, V_y, and P represent velocities in the x-direction, velocities in the y-direction, and pressure, respectively. Term F is force vector of fluid domain, where F_x and F_y are forces in the x-direction and forces in the y-direction.

Figure 2 shows a schematic diagram of a rectangular particle immersed in the Poiseuille flow and the boundary condition of the fluid domain. The Poiseuille flow profile is incorporated on the inlet. The do-nothing boundary condition is applied to the outlet. The non-slip boundary condition is incorporated on the top of the fluid domain, the bottom of the fluid domain, and the surface of the rectangular particle. A pressure boundary condition on the outlet is set to equal to zero to avoid singularity in the calculation.
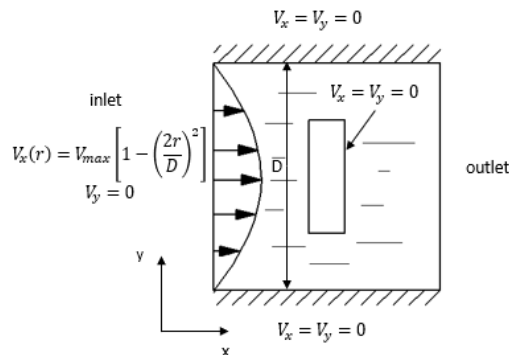

Figure 2: A rectangular particle is immersed in the Poiseuille flow.

The distributions of the velocity, distributions of the pressure, and distributions of the force in the fluid domain are obtained by solving Eq. (3.6). Only the data on the interface between the fluid domain and the rectangular particle is useful and is extracted from those results. To meet the requirements of compatibility, i.e., the velocity and the force on the interface are equivalent on both domains, results of velocities and forces on the interface of the fluid domain will be passed to the particle solver to calculate the motion of the particle.

3.2   Multi-Particle Motion

Since large displacement, large rotation, and large deformation are predicted when particles immersed in the flow, the particle's motion is treated as a non-linear geometric dynamic problem. The particle is modeled in a two-dimensional domain. Total-Lagrangian (TL) incremental finite element method can deal with the non-linear geometry. Linear material defines the property of the particle. Bathe method, a time integration scheme, integrates the semi-discrete equation resulted from the Total-Lagrangian method over the time domain.

Total-Lagrangian method measures and calculates everything on the initial referential configuration. Displacements are obtained step by step. Using the virtual work and the energy conservation obtains the governing equation of the particle in the current configuration, as shown in Eq. (3.7) [9].

$$\delta W = \int_{^2\Omega} {}^2\sigma : \delta({}_2e)d\ ^2\Omega - \delta(\ ^2R) = 0 \tag{3.7}$$

Here, δW is the virtual work of the entire particle which should be equal to zero as the energy conservation. Index '2', both in superscript and subscript, indicates the configuration: current configuration. σ represents the Cauchy stress. $\delta(\ _2e)$ is the virtual linear engineering strain increment. $\delta(\ ^2R)$ is the virtual work of the external forces. The Second Piola-Kirchhoff (2PK) stress 'S' and the Green Lagrangian strain 'E' are utilized to convert Eq. (3.7) from the current configuration to the referential configuration, as shown in Eq. (3.8).

$$\int_{^0\Omega} {}_0S : \delta({}_0\varepsilon)d\ ^0\Omega + \int_{^0\Omega} {}^1S : \delta({}_0\eta)d\ ^0\Omega = \delta({}_0^2R) - \delta({}_0^1R) \tag{3.8}$$

Similar to the function and the position of the index used in Eq. (3.7), index '1' represents the variable in the previous configuration of the current configuration '2'. Index '0' represents the referential configuration. $\delta(\ _0\varepsilon)$ is the virtual work of the linear term of the strain. $\delta(\ _0\varepsilon)$ is the virtual work of the nonlinear term of the strain. $\delta({}_0^2R)$ is the external force virtual work in the current configuration. $\delta({}_0^1R)$ is the elastic potential energy generated by the virtual work in the previous configuration. Equation (3.8) can be simplified to a matrix form, Eq. (3.9). Here, K_T is the tangent stiffness matrix of the particle. U is the displacement of the particle. ${}_0^2F_{External}$ and ${}_0^1F_{Internal}$ correspond to the $\delta({}_0^2R)$ and $\delta({}_0^1R)$, respectively.

$$K_T U = {}_0^2F_{External} - {}_0^1F_{Internal} \tag{3.9}$$

To include the inertia and the energy dissipation of the particle, the mass matrix, and the damping matrix are calculated. Since the mass conserves through different configurations, the mass of the particle in the referential configuration is equal to the mass of the particle in the further configurations. In Eq. (3.10), we calculated the mass matrix of the particle in the referential configuration. ρ_s represents the density of the particle. In Eq. (3.11), the Rayleigh proportional damping provides an empirical way to involve the energy dissipation of the particle. Weighting coefficient α and β result from the natural mode of the system combining with a given damping ratio [2].

$$M = \int_{^0\Omega} \rho_s d\ ^0\Omega \tag{3.10}$$

$$C = \alpha M + \beta K \tag{3.11}$$

A second order ordinary differential equation can be constructed. A governing equation with two particle case is

$$\begin{bmatrix} M^1 & 0 \\ 0 & M^2 \end{bmatrix} \begin{Bmatrix} \ddot{U}_{(i)}^1 \\ \ddot{U}_{(i)}^2 \end{Bmatrix} + \begin{bmatrix} C^1 & 0 \\ 0 & C^2 \end{bmatrix} \begin{Bmatrix} \dot{U}_{(i)}^1 \\ \dot{U}_{(i)}^2 \end{Bmatrix} + \begin{bmatrix} K_{t\ (i-1)}^1 & 0 \\ 0 & K_{t\ (i-1)}^1 \end{bmatrix} \begin{Bmatrix} U_{(i)}^1 \\ U_{(i)}^2 \end{Bmatrix} = \begin{Bmatrix} {}_0^2F_{external}^1 - {}_0^1F_{internal}^1(U_{(i-1)}^1) \\ {}_0^2F_{external}^2 - {}_0^1F_{internal}^2(U_{(i-1)}^2) \end{Bmatrix} \tag{3.12}$$

Superscript 1 and 2 on the top right corner indicates the number of the particles. The 'dot' above the displacement U indicates the order of time derivative. Tangent stiffness matrix $K_t(U_{(i-1)})$ refers that the motion of the particles is a non-linear problem. The Newton-Raphson iteration method is used to solve the non-linear equation. Subscripts i and $i-1$ indicate the order of the iteration. ${}_0^2F_{external}$ and ${}_0^1F_{internal}$ represent external forces on the current configuration and the internal forces stored from the previous configuration.

Bathe method [1] has two sub-steps. In the first half-time step, displacements and velocities of the particle are calculated according to the Newmark trapezoidal rule. In the second half-time step,

displacements and velocities of the particle are calculated according to the three-point Euler backward method.

Only the displacements and the velocities on the nodes of the particle's surface are needed. The displacement of the particle changes the geometry of the interface. We utilized the displacements of the particle to update the mesh of the fluid domain, which meets a requirement of the geometric compatibility in the coupling. The velocities on the particle's surface in Eq. (3.6) play as the essential boundary conditions of the fluid calculation, which meets a requirement of the kinematic compatibility in the coupling.

3.3 Explicit Partitioned Coupling Strategy

Solutions of the fluid and the particle have been introduced in the previous sections independently. To couple those two solutions together, we derived an explicit coupling method. Three coupling compatibilities including geometric compatibility, kinematic compatibility, and dynamic compatibility, need to be satisfied by handling the displacements, the velocities, and the forces appropriately between the two domains. Figure 3 shows an entire coupling scheme schematic diagram.
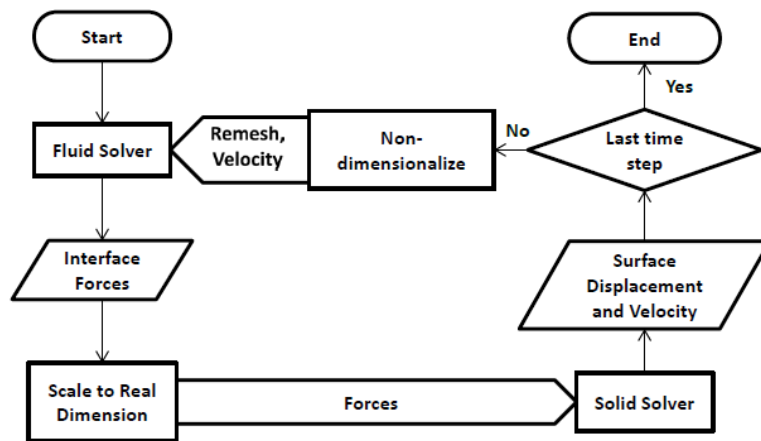

Figure 3: Explicit partitioned coupling scheme flowchart.

The fluid domain was solved first. We extracted the forces on the interface from solutions of the fluid solver. Since the fluid domain was written in the dimensionless form and the particle dynamic equation was formulated with the physical unit without dimensionless, before delivering the forces the fluid exerting on the particle to the solid solver to solve motions of the particle, the dimensionless forces need to be scaled to the dimensional forces.

To meet the requirement of dynamic compatibility, forces sourced from the fluid domain are incorporated into Eq. (3.12) as the natural boundary condition of the solid solver. Then, the solid solver is marched forward one time-step. Velocities and displacements on the particle's surface are calculated. Before delivering the velocities and the displacements from the solid solver to the fluid solver, the velocities and the displacements are translated into dimensionless data.

To meet the requirement of the kinematic compatibility, after re-mesh, the velocities on the surface of the particle are incorporated to the fluid domain on the matched node as the essential boundary condition. A coupling mainly takes places between two governing equations: Eq. (3.6) and Eq. (3.12). Figure 4 illustrates the coupling scheme from a perspective of the governing equations.
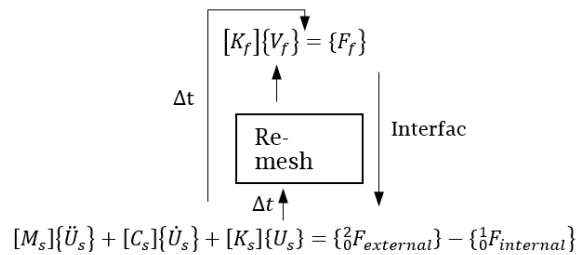
$$\Delta t \left\uparrow \begin{array}{c} [K_f]\{V_f\} = \{F_f\} \\ \\ \boxed{\begin{array}{c} \text{Re-} \\ \text{mesh} \end{array}} \quad \text{Interfac} \\ \\ \Delta t \end{array} \right.$$

$$[M_s]\{\ddot{U}_s\} + [C_s]\{\dot{U}_s\} + [K_s]\{U_s\} = \{^2_0 F_{external}\} - \{^1_0 F_{internal}\}$$

Figure 4: Explicit partitioned coupling scheme between two governing equations.

3.4 Mesh

To meet the requirement of geometric compatibility, a mesh tool named 'Distmesh [7]' is applied to re-mesh the fluid domain according to the result of the new geometry of the particle's surface. Remesh is needed every coupling step. We applied the quadrilateral element for the particle and a 6-node triangular element for the fluid domain. Both elements are the quadratic element. The apex of the element of each domain matches to each other, as shown in Figure 5. There is a small gap between the midpoints for a pair of matched elements. Only the accuracy of the midpoint is influenced. Although a deformed particle generates curved side of a quadrilateral element, the error caused by the gap is ignored. It is easy to transfer the data between to domain over the matching.
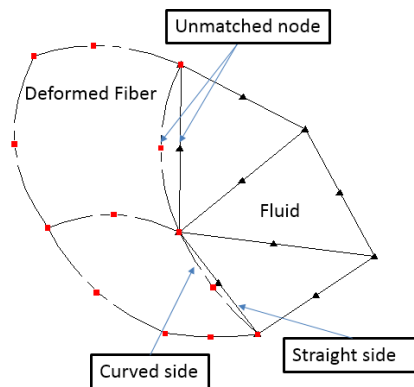

Figure 5: Matching element on the interface between two domains.

The derived method is a mesh-based method, we cannot deal with the contact of two immersed particle by far. Two particles approaching each other too closely also causes low mesh quality which will lead to inaccurate calculations. Those are limitations of the derived method for simulations of the flow-induced multi-particle.

4 SIMULATION AND DISCUSSION

All simulations were programed using the MATLAB. Simulations were running on a computer with hardware Intel(R) Core(TM) i7-8550U CPU @ 1.80GHz, 16GB RAM, and 500GB SSD.

4.1 Validation with the Jeffery Theory

The derived method is validated with the Jeffery theory (2.1). An elliptic particle immersed in an unbounded double Couette flow is simulated. A realistic way to realize the unbounded flow domain

is to set the dimension of the flow domain being 40 times larger than the dimension of the elliptic particle. In this case, the boundary effect is avoided. Mesh of the elliptic particle and the fluid domain are shown in Figure 6. Elliptic particle's axis ratio $re = 3$, density is $1300\ kg/m^3$, Young's Modulus is $37 \times 10^9\ Pa$, and damping ratio is 0. The fluid's viscosity $v = 17\ (N \cdot s)/m^2$, which was applied in the Stover's experiment [11], wall speed $V_c = 0.027\ m/s$, flow shear rate $\dot{\gamma} = 0.15\ (1/s)$. Time step size $\Delta t = 0.025s$.

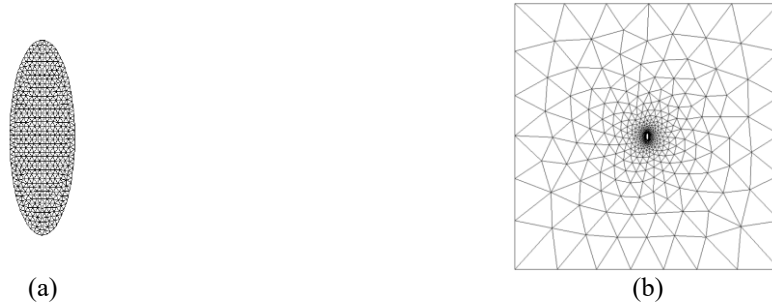(a)   (b)

Figure 6: Mesh of the simulation used for validation. (a) Mesh of an ellipsoidal fiber. (b) Mesh of the fluid domain.

Angle vs. time plot of the simulation in Figure 7 shows that the plot generated by the simulation is nicely match with the plot calculated from the Jeffery theory, which validates that the derived method has the capability of simulating flow induced particle motion problem accurately. It took 30 hours to simulate 1 min particle behaviors where 24 hours were spent to mesh. The computing speed is limited by a small time step size needed to ensure stability of the simulation.
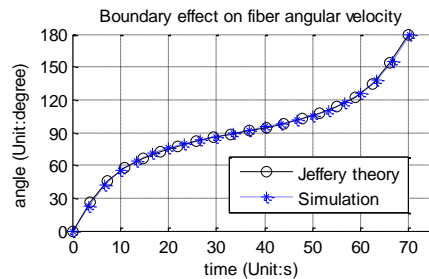

Figure 7: Comparison between results of Jeffery's theory and simulation with the derived computational method.

4.2   Shape and Aspect Ratio Effect

This section presents the effect of particle's shape and aspect ratio on the particle motion with simulations. In each case a single particle is immersed in the fluid domain. First, we show the different behaviors of flow induced elliptic particle and rectangular particle. They are immersed in the same condition of fluid domain separately. Both axis aspect ratio is 3. The only difference is their shape. Other parameters of particles and fluid are same as that applied in the Section 4.1. Figure 8 (a) compares angle vs. time plot of two different particles. It shows that the elliptic particle's rotation is slower than that of the rectangular particle immersed in the same condition of the double Couette flow.

The comparison of rectangular shape particle with axis aspect ratio 3 and 9 is also investigated. The only difference of two particles is the axis aspect ratio. Other parameters are same as those used in Section 4.1. Figure 8 (b) plots angle vs. time diagram of two particles immersed separately in the same condition of the double Couette flow. Curves illustrates that a large axis aspect ratio particle's rotation is slower than a relatively small axis aspect ratio particle with same shape.

Those conclusions from simulation can be supported by Stover's experiments observation [11]. Simulations of elliptic particle and rectangular particle with two different axis aspect ratio at several time point successively are shown in Figure 9.
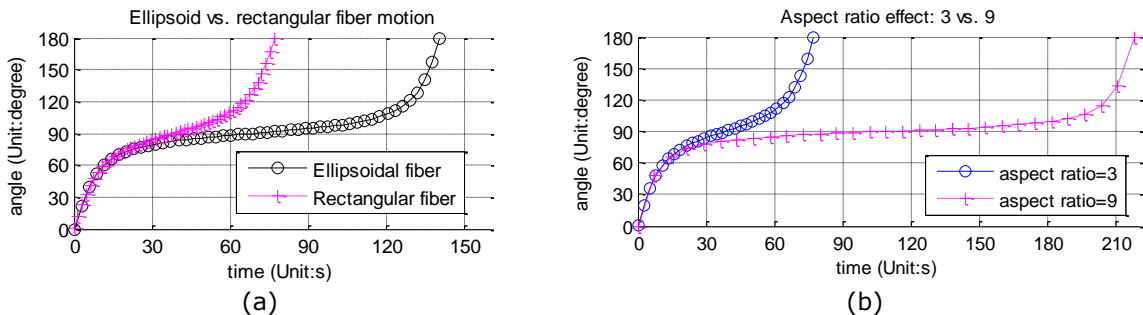

(a)   (b)

Figure 8: Angle vs. time plot. (a) Ellipsoidal fiber and Rectangular fiber. (b) Rectangular fiber with axis aspect ratio 3 and 9.
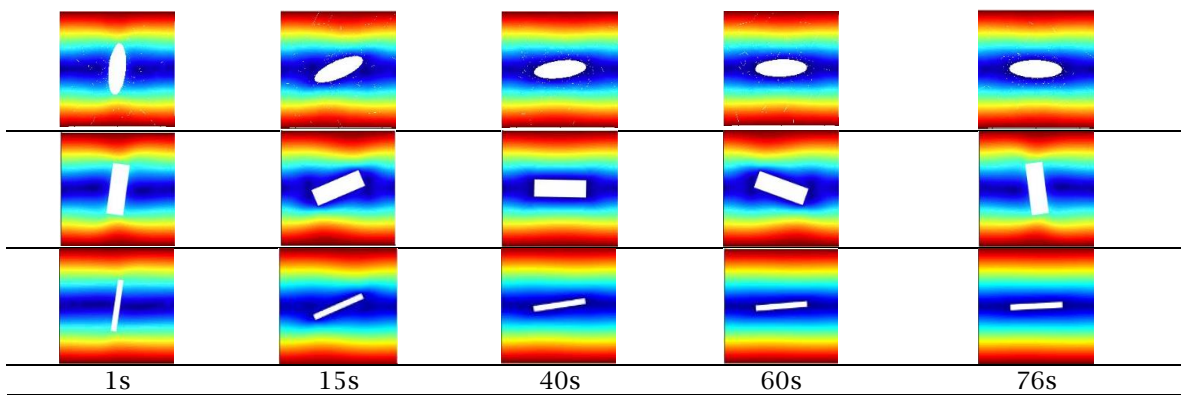

| 1s | 15s | 40s | 60s | 76s |

Figure 9: Comparison of rectangular and ellipsoidal particle position at several time points in sequence.

The 1 minute simulation of the elliptical particle took 9.3 hours, where the meshing took 4.6 hours. The 1 minute simulation of the smaller axis aspect ratio rectangular particle took 1.5 hours, where the meshing takes 0.7 hours. The 1 minute simulation of the larger axis aspect ratio rectangular particle took 1.6 hours, where the meshing took 0.8 hours.

4.3 Three Particles Immersed in the Double Couette Flow

To simulate how the existence of particle influences each other, a setup of three particles diagonally immersed in the double Couette flow was simulated. A schematic diagram of the simulation is shown in Figure 10. Parameters of the simulation are listed in Table 1. Four cases were simulated, where three particles are initially placed in different distances (i.e., $3.5\,mm$, $4\,mm$, $4.5\,mm$, and $5\,mm$) between each other in the vertical direction.
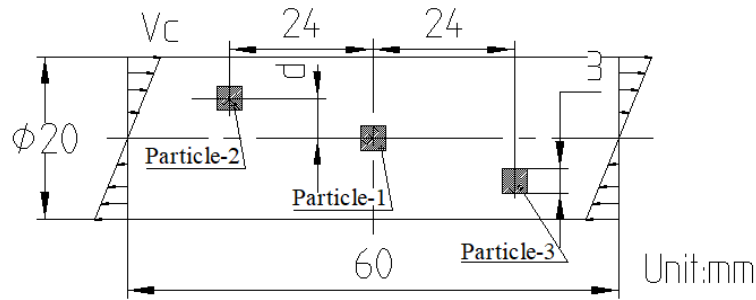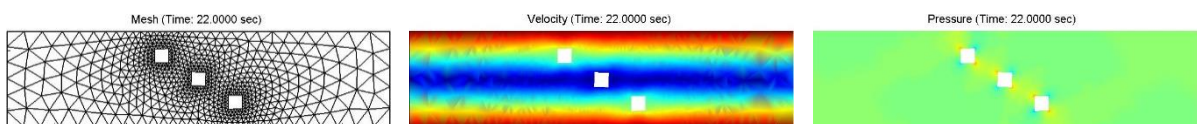
Figure 10: Simulation of three particles immersed in the double Couette flow.

	Particle-1	Particle-2	Particl-3
Type of flow	Double Couette		
Viscosity $(N \cdot s)/m^2$	17		
Fluid domain height:	2h = 0.02 m		
V_c (m/s)	$V_c = 1.5$ mm/s		
Shear rate: $\dot{\gamma}$ (1/s)	$\dot{\gamma} = 0.15\ (1/s)$		
Fiber density ρ_s	$\rho_s = 1300\ \text{kg/m}^3$		
Long axis length	Square particle: a = 3 mm		
Fiber ratio: re	re = 1		
Time step Δt (s)	Δt = 0.05		
Young's Modulus: E	37e9 (Pa)		
Damping ratio: ζ	ζ = 0		
Distance: d (mm)	3.5, 4.0, 4.5, 5.0		

Table 1: Parameters of simulations of three particles diagonally immersed in the double Couette flow.

The result of case of each particle keeping $5\ mm$ distance is presented to illustrate the flow-induced multi-particle motion as shown in Figure 11. From $22\ sec$ to $42\ sec$, flow induced three particles drift closer and then apart away. Figure 8 shows the displacements of three particles in the vertical direction in all four cases. The changing of displacement in the vertical direction of the particle on the top and the particle on the bottom shows that the existence of other particles affecting the motion of each other.

Figure 12 shows that particle-1 which was placed in the center at the beginning did not displace in the vertical direction obviously. Curves of motions of particle-2 and particle-3 in the vertical direction show symmetry in all four cases with different initial distances between particles. Particle-2 and particle-3 move slightly close to the particle-1 in the vertical direction when they approximate to the particle-1 in the horizontal direction. Then, they repel each other to the largest distance in the vertical direction when three particles aligned vertically. After that, particles tend to move closer again vertically when they depart horizontally. Finally, particle-2 and particle-3 recover to their initial vertical position after departing far away from each other. This numerical experiment shows flow-induced multi-particle motion, and reveal how particles influence the motions of each other in the direction vertical to the flow shear direction.
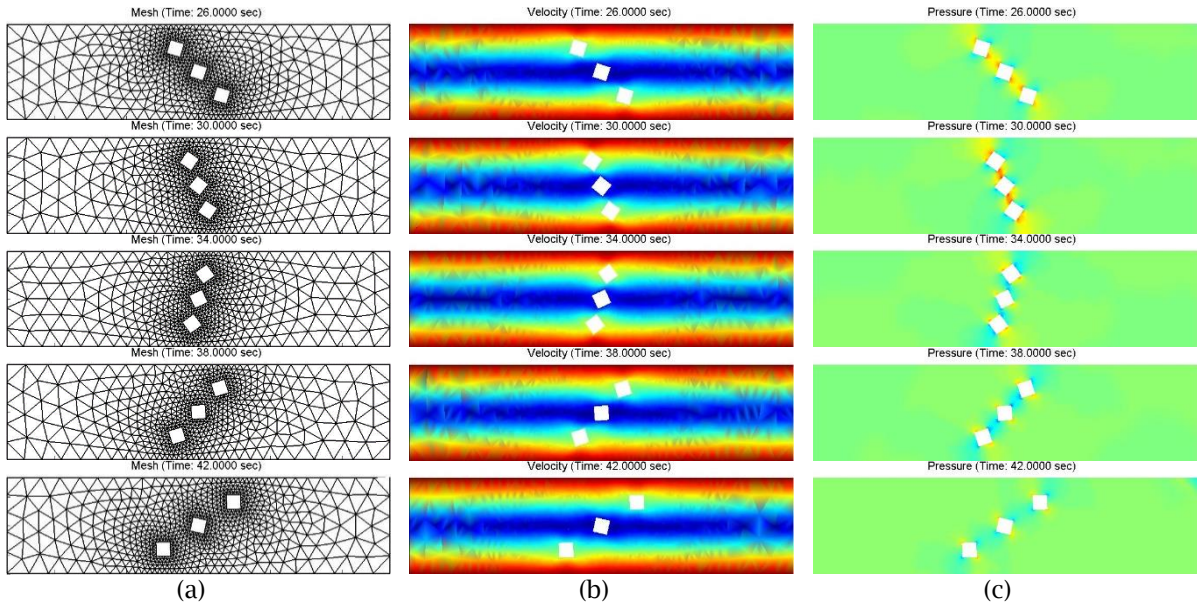
Figure 11: Results of simulation of three particles diagonally initialized arranged in the double Couette flow. (a) Mesh; (b) Velocity distribution; (c) Pressure distribution.
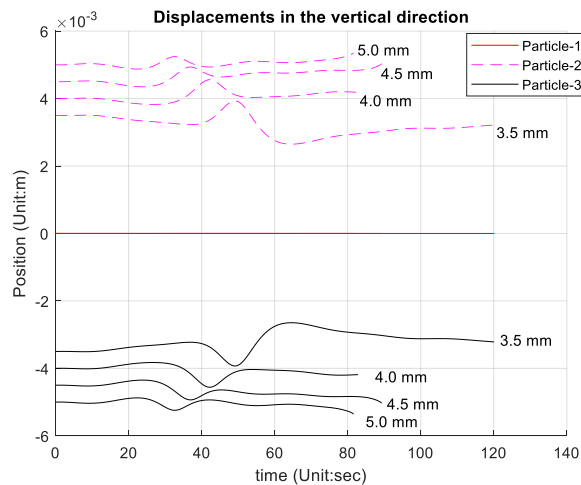

Figure 12: Displacements of three particles in the vertical direction with different initial distances between each particle.

It took 4 hours to simulate 1 minute of three particles motion in average, where 3 hours 40 minutes were spent for mesh and re-mesh.

5 CONCLUSION

For solving flow-induced multi-particle motion problem, a finite element based partitioned coupling method is presented in this paper. Stokes equation is the governing equation of the fluid domain which is solved by the mixed finite element method. The particle is modeled as a non-linear geometric dynamic problem, which is solved by the Total-Lagrangian incremental finite element

method and the Bathe time integration method. The explicit coupling strategy is developed to couple two domains. A mesh tool 'Distmesh' is applied to mesh and remesh the fluid domain at each coupling step. The derived method is validated by comparing simulation results with the Jeffery theory. Behaviors of different geometry and aspect ratio of particles are compared with simulation. Results of simulation of three particle initially diagonally immersed in the double Couette flow is discussed. The simulation revealed how the motions of particles are influenced by each other. Particles tend to attract each other when they are nearby each other in a certain area horizontally. The derived method is applied in two-dimensional domain in this study. The fluid structure coupling strategy and solver can be applied in the three dimensional domain. For scalability, the derived method is able to simulate large scale problem, such as lumber's motion in the river. The method is capable to simulate large and heavy objects immersed in the flow. Low Reynolds number is required for any scale of problems.

Xiaobo Peng, http://orcid.org/0000-0002-0498-7194
Diwei Zhang, https://orcid.org/0000-0003-0250-7676
Dongdong Zhang, http://orcid.org/0000-0001-9471-1628
Lai Jiang, https://orcid.org/0000-0003-2870-8011

REFERENCES

[1] Bathe, K. J.: Conserving energy and momentum in nonlinear dynamics: a simple implicit time integration scheme, Computers and Structures, 85(7–8), 2007, 437–445. https://doi.org/10.1016/j.compstruc.2006.09.004
[2] Burnett, D. S.: Finite Element Analysis: From Concepts to Application, Addison-Wesley Publishing Company, Whippany, New Jersey, 1987.
[3] Donea, J.; Huerta, A.; Ponthot, J.; Rodr, A.: Arbitrary Lagrangian–Eulerian methods, Encyclopedia of Computational Mechanics, 1999, 1–25. https://doi.org/10.1002/0470091355.ecm009
[4] Folgar, F.; Tucker, C. L.: Orientation behavior of fibers in concentrated suspensions, Journal of Reinforced Plastics and Composites, 3(2), 1984, 98–119. https://doi.org/10.1177/073168448400300201
[5] Ho, B. P.; Leal, L. G.: Inertial migration of rigid spheres in two-dimensional unidirectional flows, Journal of Fluid Mechanics, 65(2), 1974, 365–400. https://doi.org/10.1017/S0022112074001431
[6] Jeffery, G. B.: The motion of ellipsoidal particles immersed in a viscous fluid, Proceedings of the Royal Society A: Mathematical, Physical and Engineering Sciences, 102(715), 1922, 161–179. https://doi.org/10.1098/rspa.1922.0078
[7] Oersson, P.-O.; Edelman, A.; Strang, G.: Mesh Generation for Implicit Geometries, Massachusetts Institute of Technology, 2005. http://persson.berkeley.edu/thesis/persson-thesis-color.pdf
[8] Peskin, C. S.: The immersed boundary method, Acta Numerica, 11, 2002, 479–517. https://doi.org/10.1017/S0962492902000077
[9] Reddy, J. N.: An Introduction to Nonlinear Finite Element Analysis, Oxford University Press (Vol. 1), Oxford, UK, 2004. https://doi.org/10.1093/acprof:oso/9780198525295.001.0001
[10] Reddy, J. N.; Gartling, D. K.: The Finite Element Method in Heat Transfer and Fluid Dynamics (Third Edition), CRC Press, New York, NY, 1985.
[11] Stover, C. A.; Cohen, C.: The motion of rodlike particles in the pressure-driven flow between two flat plates, Rheologica Acta, 29(3), 1990, 192–203. https://doi.org/10.1007/BF01331355
[12] Zhang, D.; Peng, X.; Zhang, D.: Flexible fiber motion in fiber-reinforced composite material processing, in the Proceedings of the ASME International Mechanical Engineering Congress and Exposition, Pittsburgh, Pennsylvania, November 9-15, 2018. https://doi.org/10.1115/IMECE2018-86440.